Supporting Information

Defective blue titanium oxide induces high valence of NiFe-(oxy)hydroxides over heterogeneous interfacial towards high OER catalytic activity.

Tingxi, Zhou[a,†], Yifei Yang[a, †], Yike Jing[a], Yuling Hu[a], Fei Yang[a], Wei Sun[a,*] and LeiLei He[b,*]

a. Key Laboratory of Agro-Forestry Environmental Processes and Ecological Regulation, School of Ecology and Environment, Hainan University, Haikou,570228, China.

b. Zhejiang Provincial Key Laboratory of Water Science and Technology, Yangtze Delta Region Institute of Tsinghua University, Zhejiang, Jiaxing 314006, P.R. China

Table of Contents

1. Experiment Section:

1.1 Materials

Here, a commercial titanium foil with a thickness of 0.1 mm was used as a substrate, and the titanium foil was cut to the size required for our experiments. Ethanol (C_2H_5OH), oxalic acid ($C_2H_2O_4$) nickel sulfate hexahydrate ($NiSO_4 \cdot 6H_2O$, ≥98.5%), iron sulfate hexahydrate ($FeSO_4 \cdot 7H_2O$, ≥99%), potassium hydroxide (KOH) were all purchased from Maclin. The ultrapure water (18.25 MΩ cm) was prepared from the laboratory. All chemicals used in the experiments were of analytical grade and without any additional purification.

1.2 Synthesis of NiFe/B-TiO_x

First, commercial Ti was submerged in an aqueous ethanol solution for about 30 minutes to remove oil stains from the surface of the Ti foil. The pre-treated Ti foil was placed in a 10% oxalic acid solution heated to 75 °C and kept for about two and a half hours, when the surface of the Ti foil was change from smooth to rough, and from a glossy to a light gray color, that is the etched Ti.

Then, the surface of etched Ti was oxidized in 1M KOH electrolyte using an electrochemical workstation under three-electrode system, where the etched Ti foil was cut to a size if 0.5×2 cm as anode, and Pt sheet with a size of 1×1 cm was used as the cathode. The distance between the anode and the cathode was controlled be about 3 cm. The potential for Ti oxidizing was subjected to 1.5 V for to form B-TiO_x. After that, the Ti foil was washed by ultrapure water and keep in the nitrogen-treated ethanol solutions, this step is to ensure that the surface is not oxidized.

For the NiFe/B-TiO_x, B-TiO_x and Pt were used as cathode and anode, respectively. The electrodeposition electrolyte contains 0.03 M $FeSO_4 \cdot 7H_2O$ and 0.1 M $NiSO_4 \cdot 6H_2O$ with a Fe/Ni molar ratio of 1/3 (Fe-poor and Ni-rich). Then, NiFe-O_xH_y was electrodeposited on B-TiO_x for about 240 s, the amount of Coulomb deposited is approximately 1 C. For preparing the NiFe/Ti and NiFe/SS (SS-stainless steels), the electrodeposition conditions are consistent with the synthesis of NiFe/B-TiO_x.

1.3 Electrochemical measurements

All electrochemical tests, including evaluations of the OER activity and stability, were carried out in a three-electrode system using CHI760E in 1 M and 6 M KOH (pH = 13.8 and 14.6) solution. The prepared samples with an area of 0.5 cm^2 were used as working electrode, and platinum foil with an area of 1 cm^2 and the standard Hg/HgO electrode were used as counter and reference electrode, respectively. The double-layer capacitances and surface electrochemical properties of different electrodes were determined by cyclic voltammetry (CV). The OER activity with *iR*-corrected (*R*-solution resistance) was investigated by linear sweep voltammetry (LSV) with a low scan rate of 5 mV s^{-1}. The solution resistances were determined by the electrochemical impedance spectroscopy (EIS) method. The EIS was conducted at 0.6 V vs. Hg/HgO with a potential amplitude of 10 mV and a frequency ranging from 1 to 10^6 Hz. The solution and transfer resistance are obtained by fitting the Nyquist plots. The OER stability was estimated by chronopotentiometry at a constant current density of 50 and 100 mA cm^{-2}. The potential versus Hg/HgO scale was converted into the reversible hydrogen electrode (RHE) scale by calibration with an equation: $E_{RHE} = E_{Hg/HgO} + E^{\theta}_{Hg/HgO}$ (0.098) + 0.0592×pH.

1.4 Material characterizations

High-pressure tape adhesion experiments were performed to describe the firmness of surface catalysts on the B-TiO_x and etched Ti. Briefly, sticking the polyimide tape on the electrode surface and then placing it in the tablet press, adjusting the different pressures and maintaining it for 10 min, after which the tape was opened to observe the catalyst contained on the surface and confirm by photo. The bulk and surface crystal structure of electrodes is investigated by X-ray diffraction (XRD) and grazing incidence XRD (GIXRD), respectively, equipped with a D/max2550 V apparatus and a Cu-Kα radiation source (λ = 1.5406) with a data recording range of 10 to 80°and a step size of 0.02°. The morphology and composition of the samples were characterized by scanning microscopy (FESEM, Verios G4 UC) combined with energy-dispersive X-ray spectroscopy (EDS). The micro-morphology was investigated by transmission electron

microscopy (TEM, Talos F200X G2). The surface compositions and elements‘ valence states were determined by X-ray photoelectron spectroscopy (XPS) with an instrument of ESCALAB 250Xi, which the energy step size of 0.05 eV to obtain high-resolution XPS spectra. All deconvoluted high-resolution XPS spectra were calibrated by C-1s at 284.8 eV. The X-ray absorption (XAS) data of the samples were recorded at room temperature in fluorescent mode using ion chambers in the Shanghai Synchrotron Radiation Facility (SSFR, beamline BL14W1, Shanghai) and National Synchrotron Radiation Laboratory (NSRL, beamline BL11U, Hefei), China. The selected electrode area is 1 cm^2 (size~1×1 cm), the spot size is set by the synchrotron radiation facility, and the angle of incidence is 30°. During measurements, the synchrotron was operated at the energy of 3.5 GeV and the current varied between 150 and 210 mA.

In this work, the following Morlet wavelet model was used:

$$\psi(t) = \frac{1}{\sqrt{2\pi}\sigma}\left(\exp(i\kappa t) - \exp(-\frac{\kappa^2}{2})\right)\exp(-\frac{t^2}{2\sigma^2})$$

Where κ and σ are the free parameters in program. The resolution between *k*-space and *R*-space is determined by the parameters of κ and σ. In the M-WT, the larger the value of κ, the higher resolution of *R*-space, which will be very close to the EXAFS spectra. In contrary, lowing the value of κ will obtain to a high resolution of *k*-space. In this work, for a high resolution of *R*-space, we used the parameters of κ and σ are the 10 and 1, respectively.

1.5 DFT calculations

All first-principle calculations were performed using the density functional theory (DFT) methodology implemented in the Vienna Ab-initio Simulation Package (VASP). The spin-polarized projector augmented wave (PAW) method[1, 2] and the Perdew-Burke-Ernzerhof (PBE)[3, 4] electron exchange-correlation functional of the generalized gradient approximation (GGA) were used in these calculations. The energy cutoff for the wave function expanding in the plane-wave basis was set to 400 eV. The energetic convergence threshold for the self-consistent field was 1×10^{-5} eV/atom. The structure optimization force threshold was set to 0.02 eV/Å. The structure optimization force threshold was set to 0.02 eV/Å. DFT+U was carried out to correct the energy of Fe and

Ni. The U-J value was set to 2.56 eV for Fe and 5.2eV for Ni. The composition of the heterojunction is composed of two-atomic-layer slabs γ-NiFeOOH (100) and four-atomic-layer Ti_4O_7 (102) slabs with a (2×1) super unit cell. A vacuum slab of 15 Å was used. The Brillouin-zone integrations was calculated using Monkaorst-Pack grids with (4×3×1) mesh for the heterojunction. The valence electronic configurations considered in this study were Ni (3*d*,4*s*) Fe (3*d*, 4*s*), O (2*p*, 2*s*), Ti (3d, 3s), K (3*p*, 6*s*) and H (1*s*). Electronic density of states (DOS) was calculated using the tetrahedron method with Blöchl corrections for pure NiFe-LDH and NiFe/B-TiO_x systems.

The Gibbs free energy profile (DFT with Hubbard-U approach (DFT + U)) of OER at two potentials (U=0 and U=1.23 V) are adopted to model the thermochemistry mechanism, the following four electrons reaction pathways is the most convenient way to proceed:

$$H_2O(l) + * \rightarrow *OH + H^+ + e \quad (1)$$

$$*OH \rightarrow *O + H^+ + e \quad (2)$$

$$H_2O(_l) + *O \rightarrow *OOH + H^+ + e \quad (3)$$

$$*OOH \rightarrow * + O_2(g) + H_+ + e \quad (4)$$

The free energy of a gas phase molecule or an adsorbate on the surface was calculated by the equation G = E + ZPE − TS, where E is the total energy, ZPE is the zero-point energy, T is the temperature in kelvin (298.15 K is set here), and S is the entropy.

2. Figures：

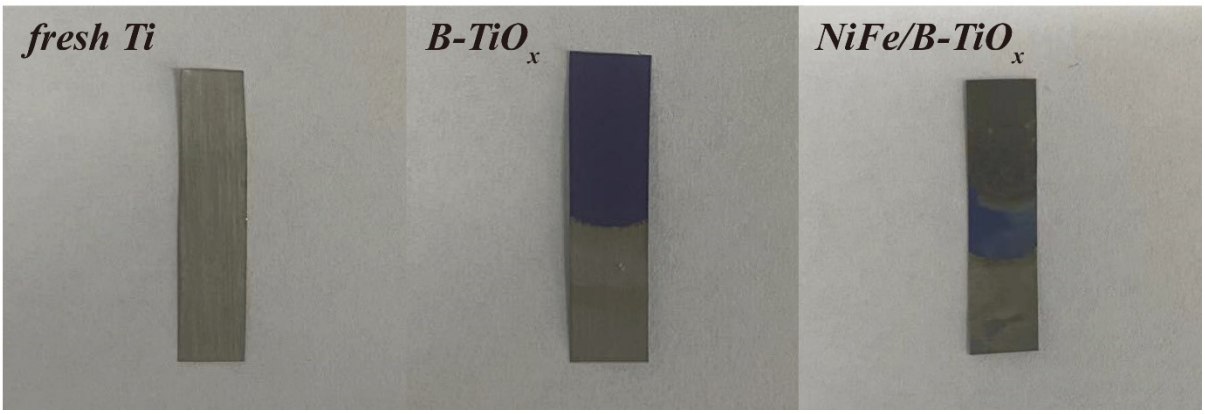

Figure S1. Optical image of fresh Ti, B-TiO_x, and NiFe/B-TiO_x.

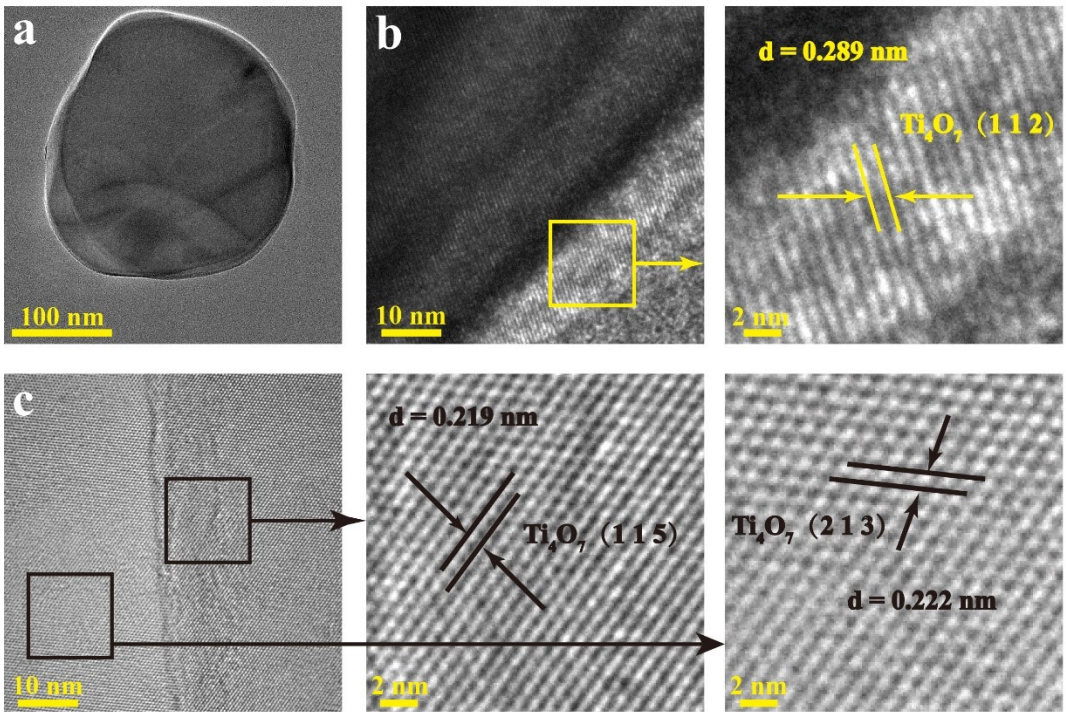

Figure S2. (a-c) TEM image of B-TiO_x under different magnifications.

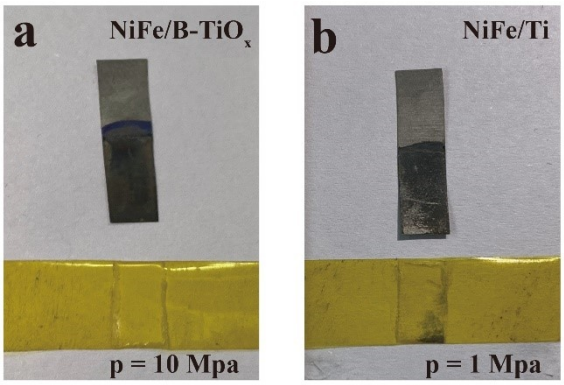

Figure S3. Optical image of (a) NiFe/B-TiO_x and (b) NiFe/Ti after the high-pressure tape adhesion experiments. The number of catalysts retained on the tape under different pressure can be used to determine the fastness of the catalysys on different substrates.

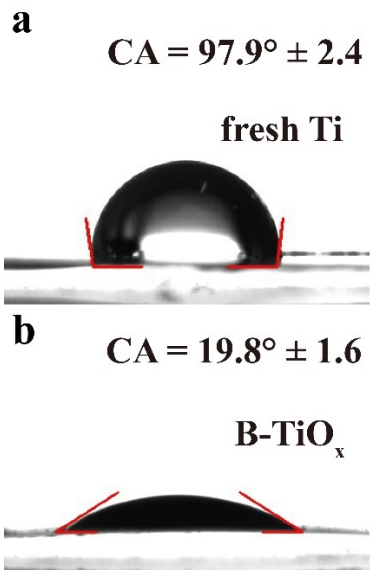

Figure S4. The measured WCA of (a) Ti and (b) B-TiO_x.

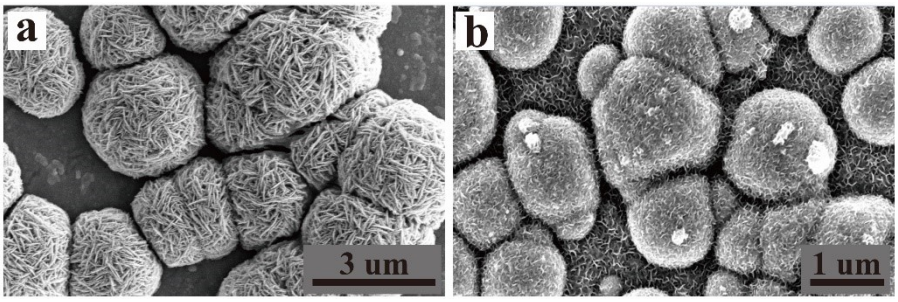

Figure S5. The SEM images of NiFe/Ti at different magnifications, which give a morphology of woolly ball that formed by the interlocking of numerous sheets.

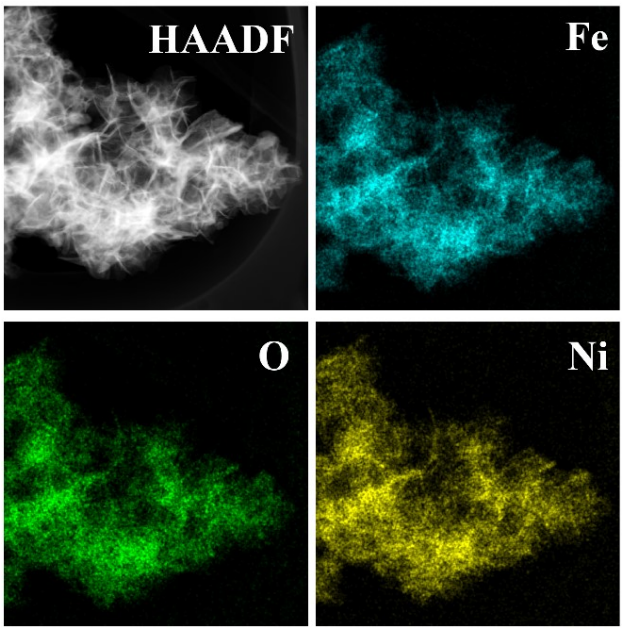

Figure S6. HAADF and EDS elemental mapping of Fe, O, and Ni of NiFe/B-TiO_x.

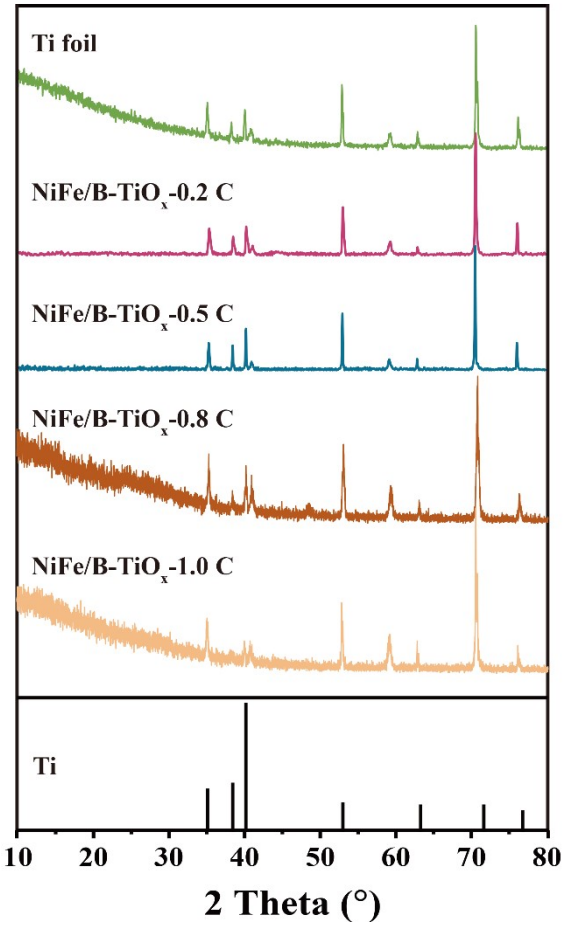

Figure S7. XRD patterns of $NiFeO_xH_y$ with different Coulomb (C).

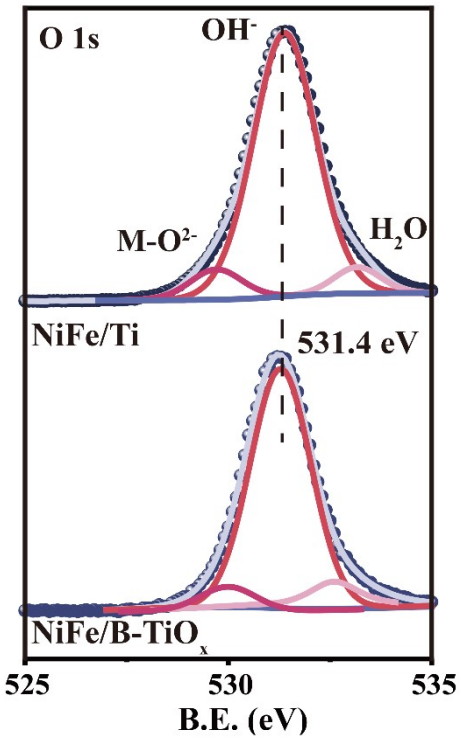

Figure S8. High-resolution XPS spectra of O-1s for NiFe/Ti and NiFe/B-TiO_x.

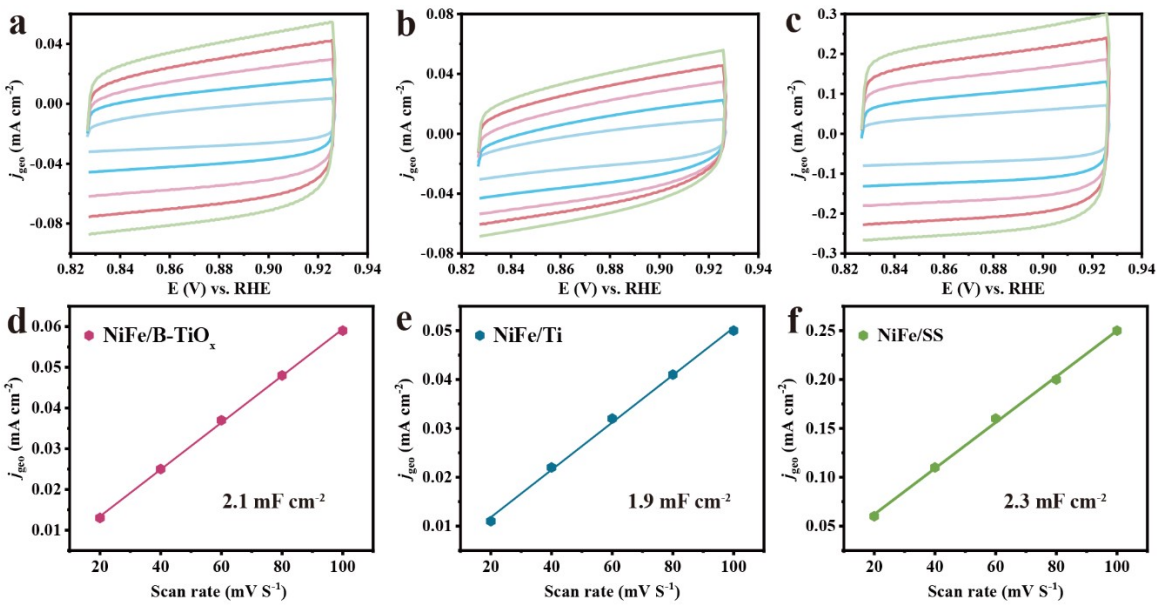

Figure S9. Cyclic Voltammetry curves of (a) NiFe/B-TiO_x (b) NiFe/Ti, (c) NiFe/SS with scan rates ranging from 20 mV s^{-1} to 100 mV s^{-1} with the interval of 20 mV s^{-1}. The scanning potential ranges from 0.82 V to 0.94 V (vs. RHE). (d-f) are the linear fitting of the i_c to the ν for NiFe/B-TiO_x, NiFe/Ti, and NiFe/SS.

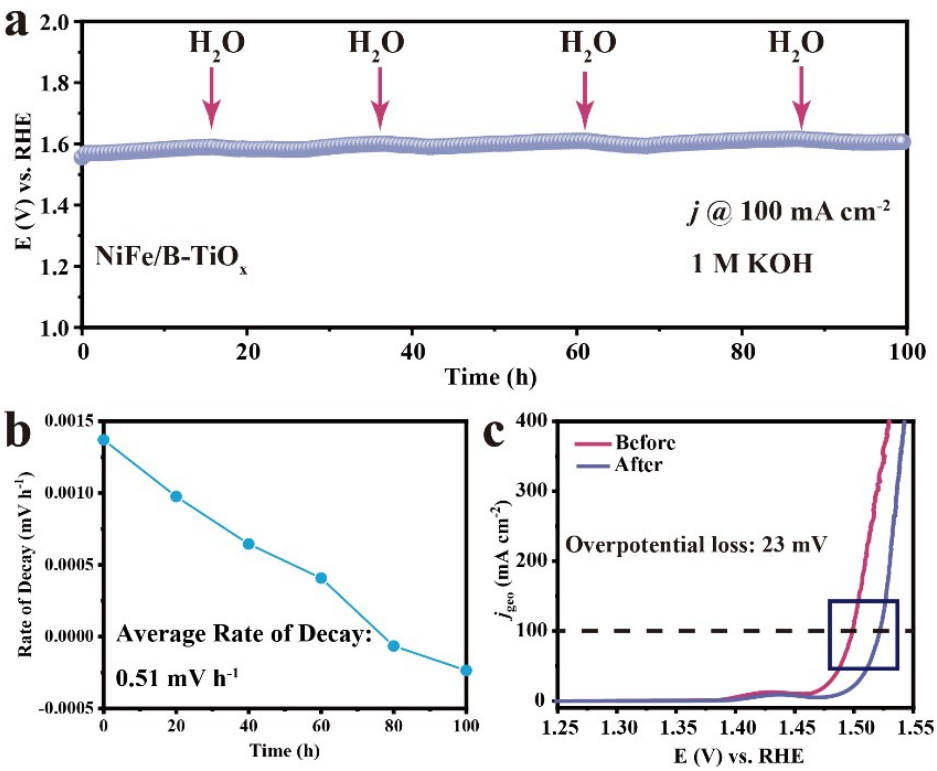

Figure S10. (a) The Chronopotentiometry curves of NiFe/B-TiO_x at the current density of 100 mA cm^{-2} for electrolysis 100 h in 1 M KOH. (b) The Rate of Decay during the electrolysis, and the average rate of decay is 0.51 mV h^{-1}. (c) the LSV curves of NiFe/B-TiO_x before and after the long-term electrolysis.

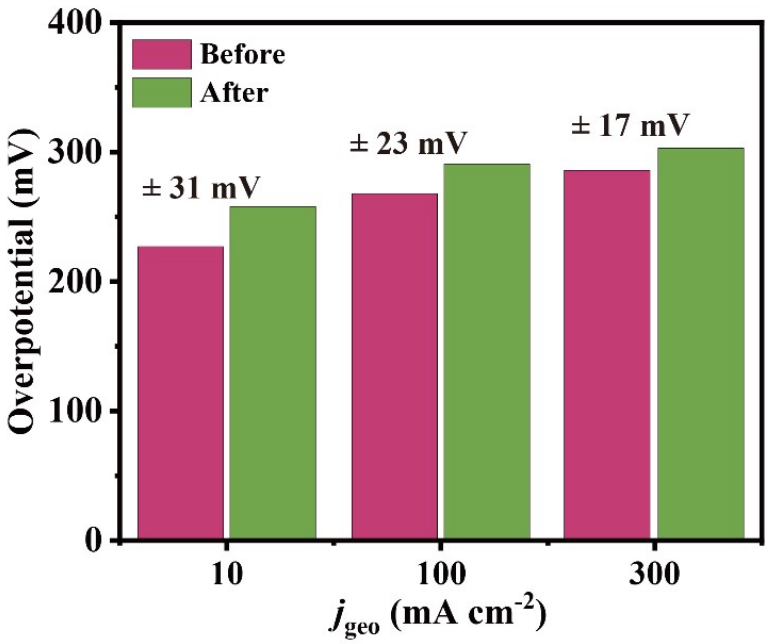

Figure S11. The overpotential comparison of NiFe/B-TiO_x before and after the long-term electrolysis under 100 mA cm^{-2} at 10, 100 and 300 mA cm^{-2}.

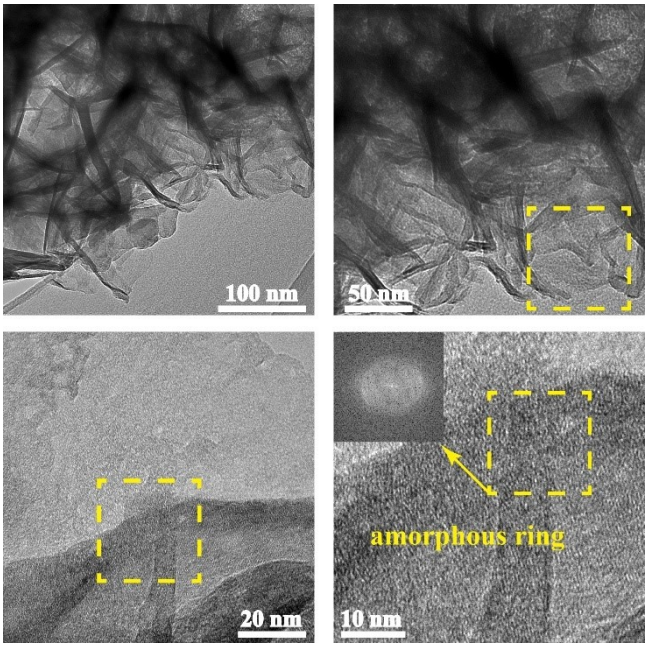

Figure S12. TEM images of NiFe/B-TiO_x after the stability.

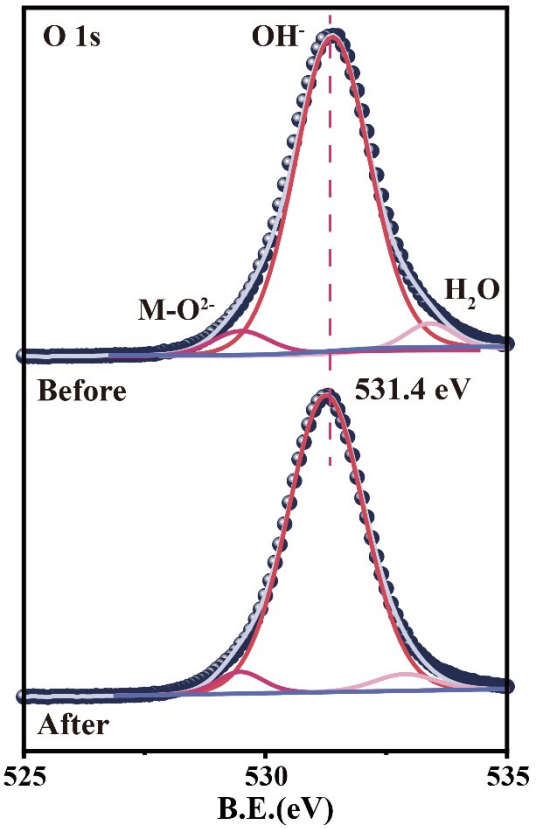

Figure S13. High-resolution XPS spectra of O-1s for the before and after OER stability of NiFe/B-TiO_x.

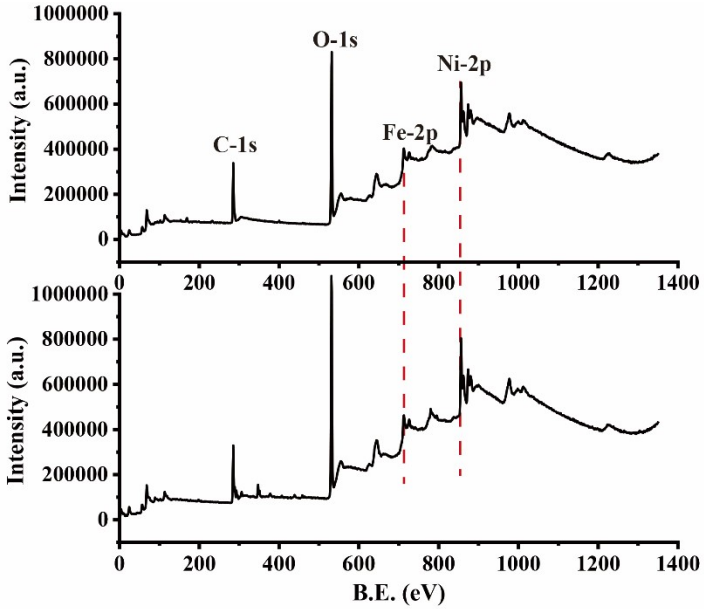

Figure S14. (a) XPS Full-spectra of NiFe/B-TiOx before and after the stability.

3. Tables：

Table S1. The obtained R_s and R_{ct} of the corresponding OER electrocatalysts from fitted Nyquist plots.

Electrocatalysts	R_s (Ω)	R_{ct} (Ω)
NiFe/B-TiO_x	2.75	1.68
NiFe/Ti	2.39	3.54
NiFe/SS	2.71	2.49

Table S2. Overpotentials (η) for OER to achieve the current density of 100 mA cm^{-2} of various substrates catalysts.

OER Electrocatalysts	Electrolyte	η (mV) at 100 mA cm^{-2}	Tafel Slope (mV dec^{-1})	References
MnO_x/NiFe-LDH/NF	1 M KOH	282	76	5
NiFe-LDH@OMC/CC	1 M KOH	296	56	6
A-NiFe-LDH	1 M KOH	320	55	7
NiFe-LDH@NiFe-Bi/CC	1 M KOH	330	96	8
Co_9S_8@NiFe-LDH/NF	1 M KOH	370	112	9
NiFe-LDH/CNT@GNR	1 M KOH	420	78	10
PLDH/GO	1 M KOH	440	52	11
NiFe/SS	1 M KOH	314	41.6	Previous work
NiFe/Ti	1 M KOH	310	42	Contrast material
NiFe/B-TiO_x	1 M KOH	268	37.5	This Work

Table S3. Elemental content quantitative analysis of XPS of NiFe/B-TiO_x before and after stability.

	Element	FWHM eV	Area (P) CPS.eV	Sensitive Factor	Atomic %	Ni/Fe ratio
Initial	Ni 2p	2.61	525814.96	20.765	17.25	2.75
	Fe 2p	5.78	239903	14.353	6.39	
After	Ni 2p	2.55	616535.21	20.765	15.21	2.56
	Fe 2p	5.82	293034.41	14.353	2.56	

4. References：

1. Notario-Estevez, A.; Kozlov, S. M.; Vines, F.; Illas, F., Electronic-structure-based material descriptors: (in)dependence on self-interaction and Hartree-Fock exchange. *Chem Commun (Camb)* **2015,** *51* (26), 5602-5.
2. Kresse, G.; Hafner, J., Ab initio molecular dynamics for liquid metals. *Physical Review B* **1993,** *47* (1), 558-561.
3. Perdew, J. P.; Wang, Y., Accurate and simple analytic representation of the electron-gas correlation energy. *Physical Review B* **1992,** *45* (23), 13244-13249.
4. Perdew, J. P.; Burke, K.; Ernzerhof, M., Generalized Gradient Approximation Made Simple. *Physical Review Letters* **1996,** *77* (18), 3865-3868.
5. Wang, Z.; Wang, C.; Ye, L.; Liu, X.; Xin, L.; Yang, Y.; Wang, L.; Hou, W.; Wen, Y.; Zhan, T., MnO(x) Film-Coated NiFe-LDH Nanosheets on Ni Foam as Selective Oxygen Evolution Electrocatalysts for Alkaline Seawater Oxidation. *Inorg Chem* **2022,** *61* (38), 15256-15265.
6. Huang, G. Q.; Zhang, C.; Liu, Z. P.; Yuan, S. S.; Yang, G. H.; Li, N., Ultra-small NiFe-layered double hydroxide nanoparticles confined in ordered mesoporous carbon as efficient electrocatalyst for oxygen evolution reaction. *Appl Surf Sci* **2021,** *565*.
7. Liu, J.; Zhou, J.; Liu, S.; Chen, G.; Wu, W.; Li, Y.; Jin, P. J.; Xu, C. L., Amorphous NiFe-layered double hydroxides nanosheets for oxygen evolution reaction. *Electrochimica Acta* **2020,** *356*.
8. Zhang, L.; Zhang, R.; Ge, R.; Ren, X.; Hao, S.; Xie, F.; Qu, F.; Liu, Z.; Du, G.; Asiri, A. M.; Zheng, B.; Sun, X., Facilitating Active Species Generation by Amorphous NiFe-B(i) Layer Formation on NiFe-LDH Nanoarray for Efficient Electrocatalytic Oxygen Evolution at Alkaline pH. *Chemistry* **2017,** *23* (48), 11499-11503.
9. Gao, X. T.; Yu, Z.; Zheng, K. X.; Yin, J. M.; Zheng, Y.; Zhu, X. M.; Dong, Y. W., Hollow Co9S8@NiFe-LDH nanoarrays supported by nickel foam for boosting the overall water-splitting performance. *Mater Lett* **2022,** *319*.
10. Yin, X.; Hua, Y. N.; Hao, W. B.; Yang, J.; Gao, Z., Hierarchical nanocomposites of nickel/iron-layered double hydroxide ultrathin nanosheets strong-coupled with nanocarbon networks for enhanced oxygen evolution reaction. *Electrochimica Acta* **2022,** *420*.
11. Xie, J. Y.; Li, C.; Niu, J. N.; Zhang, S. H.; Ou, X. M.; Feng, P. Z.; Garcia, H., Porous NiFe-LDH grown on graphene oxide towards highly efficient OER electrocatalysis. *Mater Lett* **2021,** *290*.